LoRaWAN multiple-access interference cancellation for LEO-PNT

Yago Sánchez-Costa, Daniel Egea-Roca, José A. López-Salcedo, Gonzalo Seco-Granados

Yago.Sanchez@autonoma.cat,Daniel.Egea@uab.cat, Jose.Salcedo@uab.cat, Gonzalo.Seco@uab.cat

IEEC-CERES, Universitat Autonòma de Barcelona, Spain.

***Abstract*—This paper proposes a Low Earth Orbit (LEO) Positioning, Navigation, and Timing (PNT) system leveraging LoRaWAN signals. We introduce a framework for processing LoRa transmissions in LEO scenarios, featuring a robust method for Doppler shift and time-delay estimation. To address collision-induced performance degradation caused by the ALOHA-based medium access protocol, we present an interference mitigation strategy. The system is evaluated through extensive Monte Carlo simulations, demonstrating reliable performance in single-signal conditions. However, results indicate significant performance degradation in collision scenarios. This work provides foundational insights into LoRaWAN-based LEO PNT systems and their challenges in practical deployments.**

I. Introduction

The Internet of Things (IoT) has significantly transformed various sectors, driven by advancements in low-power wide-area networks (LPWAN) such as LoRaWAN and global navigation satellite systems (GNSSs). While LoRaWAN enables long-range connectivity with minimal power consumption, its coverage remains limited by terrestrial infrastructure. On the other hand, GNSS plays a crucial role in positioning, navigation, and timing (PNT) but is often power-intensive and susceptible to interference in challenging environments. Leveraging low-Earth orbit (LEO) satellite constellations presents a promising approach to enhancing IoT connectivity and optimizing satellite-based PNT solutions [1].

Recent research has explored the use of chirp spread spectrum (CSS) signals for LEO-based PNT [2], demonstrating a significant reduction in receiver complexity compared to traditional GNSS signals [1]. Although LoRaWAN employs CSS modulation at the physical layer, these optimized PNT signal designs cannot be directly adapted to LoRaWAN due to its signal structure [3]. Previous studies have considered terrestrial positioning systems based on round-trip time (RTT) measurements [4], but this approach is unsuitable for satellite applications. More recently, the feasibility of transmitting LoRaWAN signals from LEO satellites has been investigated for communication purposes [5], yet its potential for PNT applications has not been explored.

This work introduces, for the first time (to the best of the author's knowledge), a LEO-PNT solution using LoRaWAN. It is important to note that LoRaWAN was originally designed for communication purposes so that the LoRaWAN signal processing must be modified to achieve PNT. First, we need time-delay and Doppler estimation, which can be achieved as in [1] but considering the up- and down-chirps transmitted during the LoRaWAN preamble. Second, signal detection and data demodulation can follow classical LoRaWAN processing [6]. Finally, multi-satellite access must be provided by means of ALOHA protocol, which is used in LoRaWAN [3]. Unfortunately, the use of ALOHA may produce collisions between satellites thus denying the PNT service.

This activity has been partially supported by the Catalan Government in the framework of the NewSpace Strategy of Catalonia, Grant PID2023-152820OB-I00 funded by MICIU/AEI/10.13039/501100011033 and by ERDF/EU, Grant PDC2023-145858-I00 funded by MICIU/AEI/10.13039/501100011033 and by the European Union NextGenerationEU/PRTR, and the AGAUR - ICREA Academia Program.

Various interference cancellation algorithms exist in the literature [7]–[12]. For instance, [12] introduces a de-chirp with variable amplitude that allows to cancel interference, while [8] intersects several demodulation windows and only takes the information available in every window. Unfortunately, this literature is not designed to operate on the LoRaWAN preamble, which is essential to extract time-delay and Doppler measures needed for PNT. To overcome this limitation, this study proposes a simple yet effective interference cancellation technique that allows a LoRaWAN receiver to process multiple signals arriving from different LEO satellites for PNT purposes.

The contribution of this paper is twofold. First, we propose a novel interference cancellation technique that works at LoRaWAN preamble. Second, we provide a detailed framework for signal detection, data demodulation, and measurement estimation in the context of LEO-PNT with LoRaWAN. This framework provides implementation details of signal processing algorithms and configurations needed to use LoRaWAN signals for LEO-PNT. To do so, the rest of the paper is structured as follows: First, Section II introduces the signal model. Then, Section III proposes a LoRaWAN-based LEO-PNT receiver. The results of the Monte-Carlo simulation are detailed in Section IV. Finally, Section V concludes this paper.

II. Signal model

This section presents the LoRaWAN physical layer signal structure, focusing on its chirp spread spectrum (CSS) modulation scheme.

A. Chirp signal

The physical layer of LoRaWAN, the LoRa signal, is based on chirp spread spectrum signal wirten as

$$c_k(t) = e^{j\phi_k(t)}, \tag{1}$$

where the phase $\phi_s(t)$ is defined as

$$\phi_k(t) = 2\pi \int_0^t \left(\mathrm{mod}\left[f_k + \mu u\right]_B - \frac{B}{2} \right) du. \tag{2}$$

Here, f_k denotes the starting frequency of the symbol k, B denotes the signal bandwidth, μ is the chirp rate, and $\mathrm{mod}[\cdot]_B$ corresponds to the modulo B operator. The chirp rate is defined $\mu = B/T_\mathrm{c}$ being T_c the chirp duration. Data modulation is achieved by introducing an offset in the starting frequency $f_k = k/B$.

B. LoRaWAN Signal Structure

In the LoRaWAN standard [3], each packet transmission begins with a preamble composed of three distinct sections (see Fig. 1): First, a variable number of upchirps (8 by default) used for signal detection and initial timing/frequency estimation. Second, two synchronization chirps specifically designed for network identification. Third, 2.25 downchirps that complete the preamble structure. The synchronization chirps serve the dual purpose of frame synchronization and satellite identification, while the remaining preamble

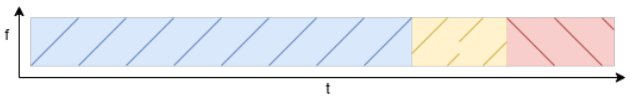

Fig. 1. LoRa preamble structure.

components (the initial upchirps and final downchirps) enable reliable packet detection and provide necessary timing and frequency correction capabilities for subsequent data demodulation, and more importantly for PNT, time-delay and Doppler measurements.

The preamble of a LoRa signal is defined as

$$s_{\mathrm{p}}(t) = \begin{cases} c_0(t), & \text{if } 0 < t < 8T_{\mathrm{c}} \\ c_{id1}(t), & \text{if } 8T_{\mathrm{c}} < t < 9T_{\mathrm{c}} \\ c_{id2}(t), & \text{if } 9T_{\mathrm{c}} < t < 10T_{\mathrm{c}} \\ c_0^*(t), & \text{if } 10T_{\mathrm{c}} < t < 12.25T_{\mathrm{c}} \end{cases} \tag{3}$$

where T_{p} is the starting time of the packet, id1 and id2 denote the 2 symbols used for network identification. The payload signal for the k-th transmitted data chirp is modeled as

$$s_{\mathrm{d}}(t) = \sum_{i=0}^{N-1} c_{k(i)}(t) \sqcap \left(\frac{t - iT_{\mathrm{c}}}{T_{\mathrm{c}}}\right) \tag{4}$$

where $k(i)$ is the symbol corresponding to the k-th chirp. The pulse function $\sqcap$ is defined as:

$$\sqcap\left(\frac{t}{T}\right) = \begin{cases} 1, & \text{if } 0 \le t \le T, \\ 0, & \text{otherwise} \end{cases} \tag{5}$$

Combining both components, a LoRaWAN packet can be expressed as

$$s(t) = s_{\mathrm{p}}(t) + s_{\mathrm{d}}(t - 12.25T_{\mathrm{c}})e^{j\theta} \tag{6}$$

where $\theta = -2\pi T_{\mathrm{c}}(\frac{\mu^2 T_{\mathrm{c}}}{32} - \frac{B}{8})$ is the phase offset introduced by the quarter downchirp (see Fig. 1). The received signal is the sum of the transmitted signals from X different satellites affected with their propagation effects and the AWGN noise of the receiver ($w(t)$):

$$r(t) = \sum_{x=1}^{X} \alpha_x s_x(t\gamma_x - \tau_x) e^{j2\pi\beta_x(t\gamma_x)} + w(t), \tag{7}$$

where $s^{(x)}$ represents the packet of the signal transmitted by the x-th satellite. On the other hand $\gamma_x = f_0/(f_0 + f_{\mathrm{D}}^{(x)})$ models the dynamic between satellite and receiver, and

$$\beta_x(t) = \beta_x + f_D^{(x)}(t_x - \tau_x) + \dot{f}_{\mathrm{D}}^{(x)}(t_x - \tau_x)^2 \tag{8}$$

The variables f_D and $\dot{f}_{\mathrm{D}}$ represent the doppler shift and doppler rate, respectively. β is a random phase offset.

Sampling at a rate of $F_{\mathrm{s}} = 2B$, the resulting discrete-time signal is $r[n] = r(t)\big|_{t=\frac{n}{F_{\mathrm{s}}}}$.

III. LEO-PNT Receiver with Interference Cancellation

In this section we propose a LoRa receiver capable of estimating the doppler shift and delay of the receiving signals both in single-signal and multiple-signal scenarios apart from demodulating the data.

A. Data Demodulation

The process of data demodulation begins with a dechirping operation, which is defined as

$$r_{\mathrm{dc}}^{(i)}[n] = r[n + T_i]c_0^*[n] \sqcap \left[\frac{n}{M}\right] = e^{j2\pi f_k n} \sqcap \left[\frac{n}{M}\right] + w[n], \tag{9}$$

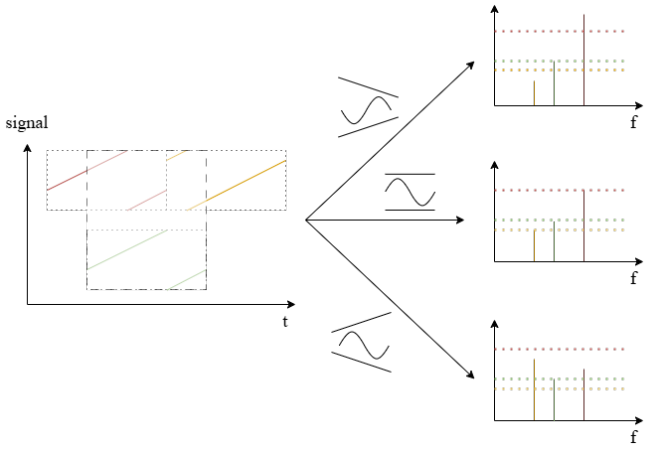

Fig. 2. Conceptual idea of the dechirping with varying amplitude chirps.

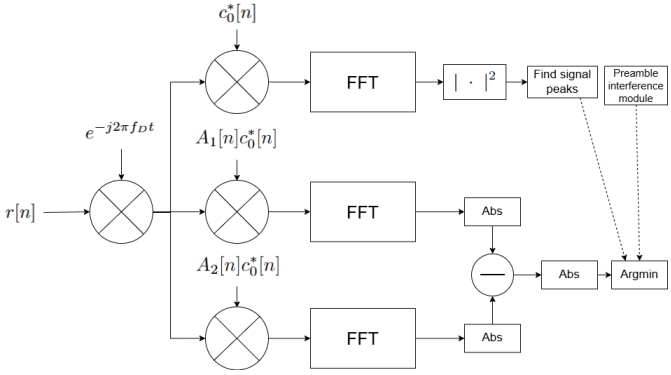

Fig. 3. Data demodulation process.

where T_i is the starting sample of the i-th symbol and M the number of samples per chirp. The discrete spectral density of the dechirped signal is:

$$R_{\mathrm{dc}}^{(i)}[m] = |\mathrm{DFT}\{r_{\mathrm{dc}}^{(i)}[n]\}|^2 = \left|\sum_{n=0}^{M-1} r_{\mathrm{dc}}^{(i)}[n] e^{-j2\pi\frac{n}{M}m}\right|^2, \tag{10}$$

where the index m denotes the samples in the discrete frequency domain. Finally, the i-th estimated symbol is

$$\widehat{k}(i) = \arg\max_m \{R_{\mathrm{dc}}[m]\}. \tag{11}$$

In the presence of interference, the basic demodulation operation is no longer viable, as interfering chirps generate additional frequency peaks that cannot be trivially separated. Consequently, only the symbols from the strongest signal at a given moment can be extracted. Inspired by [12], the idea is to exploit the desynchronized demodulating windows of interfering signals. This is achieved during the dechirping process by varying the amplitude of the downchirp, which alters the power distribution of frequencies over time. As shown in Fig. 2, the only frequency peak that remains constant is the one that is synchronized.

When no collision is detected chirps are demodulated the conventional way. Otherwise, the demodulation process when detecting a collision is depicted in Fig. 3, and it proceeds as follows. The first step in the process involves detecting all frequency peaks within the spectrum. This detection is achieved through a standard dechirping operation followed by computation of the dechirped signal's power spectral density. The noise of the spectral density of the dechirped signal will follow a central χ^2 distribution with 2 degrees of freedom and scaled by a factor $2M\sigma_n^2$ (see 10). Consequently, the detection

threshold can be fixed as:

$$h = \sigma_n^2 M \chi_2^{-1} \left((1 - P_e)^{\frac{1}{M}} \right) \tag{12}$$

where P_e is the target false alarm probability and σ_n^2 the noise variance. Two additional dechirping operations are performed using amplitude-scaled downchirps with $A_1[n] = n^2$ and $A_2[n] = (M - n)^2$. The demodulated symbol corresponds to the index minimizing $||\text{DFT}\{r_{\text{dc}}[n]A_1[n]\}| - |\text{DFT}\{r_{\text{dc}}[n]A_2[n]\}||$ among the previously calculated frequency indexes.

Note that this strategy fails when two consecutive symbols are identical. While this is not a significant issue in most cases, the preamble consists of eight consecutive identical symbols. However, during data demodulation, the time of arrival and Doppler shift of interfering signals are known, allowing the calculation of the frequency at which interference will appear after dechirping:

$$f_p = \text{mod}[\mu\tau' + \Delta f_{\text{D}}]_B, \tag{13}$$

where $\Delta f_{\text{D}} = f_{\text{D}} - f'_{\text{D}}$ is the difference in frequency offsets, and τ' is the delay between the start of the demodulating window and the beginning of the interfering upchirp. Knowing the frequencies of the preambles interferences we can discard these frequencies when demodulating.

B. Signal Detection

For signal detection and a signal's arrival time broad estimation, as proposed in [12], we correlate the received samples with an upchirp. A detection is confirmed when the correlation exceeds a threshold eigth times, with the separation equal to the chirp period. The correlation is:

$$R_x[k] = \left| \sum_{n=0}^{2M-1} r[n+k] c_0^*[n] \sqcap \left(\frac{n - M}{2M} \right) \right|^2 \tag{14}$$

Following the same logic as with signal detection, from the spectrum of the dechirped signal, peaks corresponding to signals are filtered from noise using a threshold:

$$h = \sigma_n^2 M \chi_2^{-1} \left((1 - P_e)^{\frac{1}{L}} \right) \tag{15}$$

where L is two times the length of $r[n]$ minus 1.

C. Time and Frequency Corrections

As explained in [1], the delay and frequency shift of the signal can be estimated using the dechirped signals of both an upchirp and a downchirp from the preamble. In order to mitigate the effect of interference, based on the work of [8], we propose a method that takes advantage of the deterministic nature of the preamble. To isolate the contribution of the studied signal we intersect the dechirped spectrum of the 6 interior chirps of the preamble, as they have more power.

$$R_{\text{dc}}^{+}[m] = \cap_{p=1}^{6} R_{\text{dc}}^{(p)}[m] \tag{16}$$

where $R_{\text{dc}}^{(i)}[m]$ is the FFT of the p-th preamble dechirped chirp.

And for the downchirps we select the second chirp for the same reason. So,

$$R_{\text{dc}}^{-}[m] = R_{\text{dc}}^{(11)}[m] \tag{17}$$

For a better estimation of the peaks frequencies we make an interpolation of both $R_{\text{dc}}^{+}[m]$ and $R_{\text{dc}}^{-}[m]$ using MATLAB function spline(). Then the frequencies of the dechirped isolated signal are:

$$\begin{aligned} f_+ &= \arg\max_k \{|R_{\text{dc}}^{+}[m]|^2\} \frac{B}{N} \\ f_- &= \arg\max_k \{|R_{\text{dc}}^{-}[m]|^2\} \frac{B}{N}, \end{aligned} \tag{18}$$

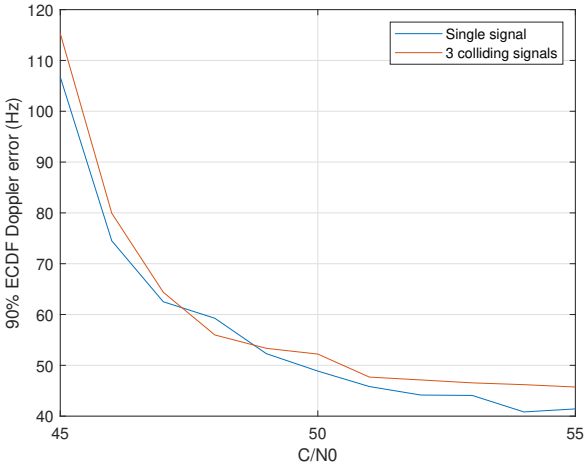

Fig. 4. Doppler shift error with respect to CN_0.

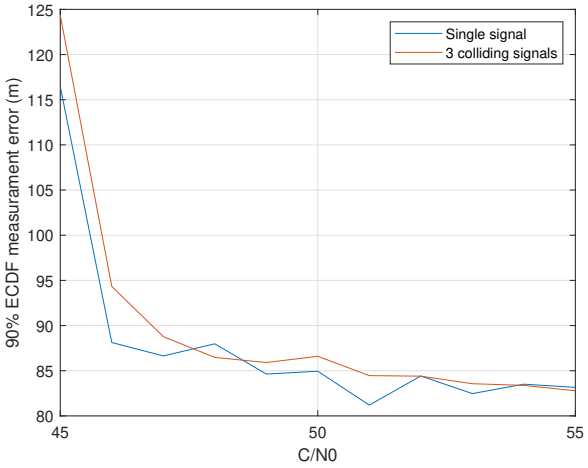

Fig. 5. Distance error with respect to CN_0.

where N is the number of samples of the dechirped spectrum after interpolation. The estimation of the Doppler shift and the time delay is based on combining the frequencies in (18):

$$\begin{aligned} \hat{\tau} &= -\frac{f_+ - f_-}{2\mu} \\ \hat{f}_{\text{D}} &= \frac{f_+ + f_-}{2}. \end{aligned} \tag{19}$$

These estimates enable: (1) downchirp-received signal alignment, (2) Doppler shift compensation, and (3) preamble interference calculation.

IV. Results

We evaluate receiver performance via Monte Carlo simulations for both single-signal and three-interferer scenarios, using parameters: SF=7, $B = 500\,\text{kHz}$, $f_0 = 868\,\text{MHz}$, 100 realizations, and $P_e = 10^{-2}$. Random Doppler shifts (max 30 kHz), Doppler rates (max 270 Hz/s), and timing offsets follow [13]. All signals maintain equal power. Key metrics include Doppler/timing estimation errors, pre-decoding BER, and signal detection rate.

Without interference cancellation techniques, signal recovery in collision scenarios is not possible, as overlapping transmissions cannot be properly separated. As observed in Fig. 4 and Fig. 5 respectively, the Doppler shift and delay (τ) estimation exhibit similar performance in both collision and non-collision cases. However,

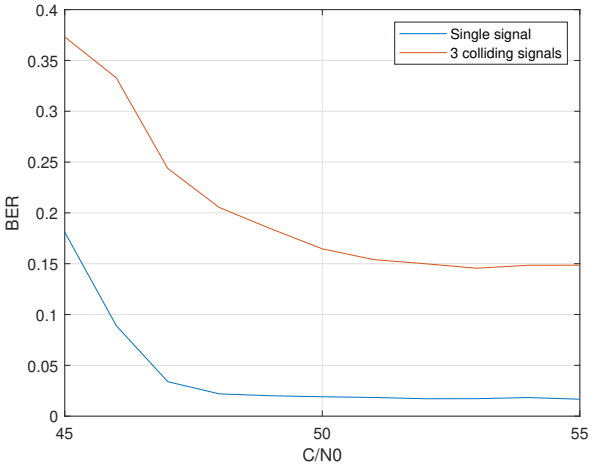

Fig. 6. Pre-decoding BER with respect to CN_0.

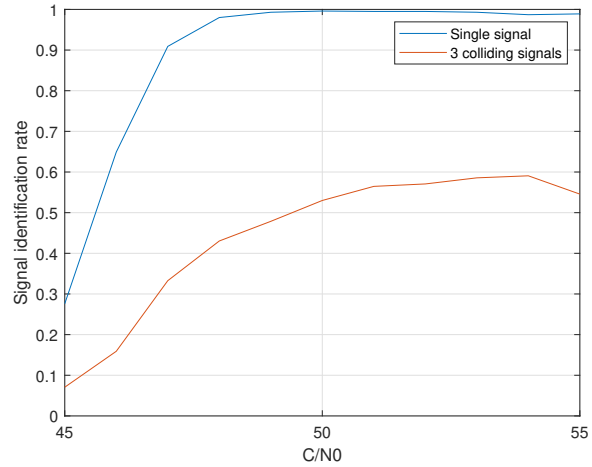

Fig. 7. Number of signals correctly detected with respect to CN_0.

the single-signal case shows a slight error in the curve, attributed to phase misalignment between chirp segments. While this issue can be mitigated using the solution for this problem proposed in [12], such a solution introduces additional computational complexity. Furthermore, the bit error rate (BER) remains significantly higher in collision scenarios as seen in Fig. 6. Lastly Fig. 7 shows the rate of signal identification, meaning that the net ID in the preamble coincides with the one sent in at least all bits except one.

V. Conclusions

This work presented a LoRa-based positioning system for LEO constellations, including signal modeling, receiver design, interference mitigation techniques, and Doppler/tau estimation. Monte Carlo simulations validated the system's performance. We tried to address the possibility of solving collision between different satellite signals.

Although the system exhibits comparable performance in Doppler shift and delay (τ) estimation under both collision and non-collision scenarios, its demodulation accuracy for information-carrying chirps remains significantly degraded in collision conditions. While this partial functionality demonstrates some utility, the marginal gains achieved do not justify the increased computational complexity required for implementation. Further optimization or alternative interference mitigation techniques may be necessary to enhance demodulation reliability without disproportionately escalating system overhead.

Future work should incorporate Doppler rate calculation, test with real signals, implement symbol accumulation for final decision-making, and explore dechirp+FFT alternatives to correlation-based processing.

References

[1] Daniel Egea, José A. López-Salcedo, Gonzalo Seco-Granados, and Emanuela Falletti. Comparison of several signal designs based on chirp spread spectrum (css) modulation for a leo pnt system. In *Proc. ION GNSS+*, pages 2804–2818, 10 2021.

[2] Daniel Egea-Roca, José A López-Salcedo, and Gonzalo Seco-Granados. Performance analysis of the pilot- and data-component of a CSS signal for LEO-PNT. *Eng. Proc.*, 54(1):35, 2023.

[3] LoRa Alliance. LoRaWAN 1.0.3 specification. Standard, LoRa Alliance, July 2018. Revision 1.0.3.

[4] Qiang Liu, XiuJun Bai, Xingli Gan, and Shan Yang. Lora rtt ranging characterization and indoor positioning system. *Wireless Communications and Mobile Computing*, 2021(1):5529329, 2021.

[5] Mohamed Amine Ben Temim, Guillaume Ferré, and Romain Tajan. A New LoRa-like Transceiver Suited for LEO Satellite Communications. *Sensors*, 22(5):1830, 2022.

[6] Thomas Ameloot, Hendrik Rogier, Marc Moeneclaey, and Patrick Van Torre. Lora signal synchronization and detection at extremely low signal-to-noise ratios. *IEEE Internet of Things Journal*, 9(11):8869–8882, 2022.

[7] Rashad Eletreby, Diana Zhang, Swarun Kumar, and Osman Yağan. Empowering low-power wide area networks in urban settings. In *Proceedings of the Conference of the ACM Special Interest Group on Data Communication*, SIGCOMM '17, page 309–321, New York, NY, USA, 2017. Association for Computing Machinery.

[8] Muhammad Osama Shahid, Millan Philipose, Krishna Chintalapudi, Suman Banerjee, and Bhuvana Krishnaswamy. Concurrent interference cancellation: decoding multi-packet collisions in lora. In *Proceedings of the 2021 ACM SIGCOMM 2021 Conference*, SIGCOMM '21, page 503–515, New York, NY, USA, 2021. Association for Computing Machinery.

[9] Shuai Tong, Zhenqiang Xu, and Jiliang Wang. Colora: Enabling multi-packet reception in lora. In *IEEE INFOCOM 2020 - IEEE Conference on Computer Communications*, pages 2303–2311, 2020.

[10] Xianjin Xia, Yuanqing Zheng, and Tao Gu. Ftrack: Parallel decoding for lora transmissions. *IEEE/ACM Transactions on Networking*, 28(6):2573–2586, 2020.

[11] Xiong Wang, Linghe Kong, Liang He, and Guihai Chen. mlora: A multi-packet reception protocol in lora networks. In *2019 IEEE 27th International Conference on Network Protocols (ICNP)*, pages 1–11, 2019.

[12] Shuai Tong, Jiliang Wang, and Yunhao Liu. Combating packet collisions using non-stationary signal scaling in lpwans. *IEEE/ACM Transactions on Networking*, 30(3):1104–1117, 2022.

[13] Cong Cao and Shenghua Zhai. The influence of leo satellite doppler effect on lora modulation and its solutio. *Journal of Physics: Conference Series*, 1883(1):012071, apr 2021.